Electron scattering mechanisms in n-type indium selenide

A. Segura, F. Pomer, and A. Cantarero
Departamento de Electricidad y Magnetismo, Facultad de Ciencias Físicas, Universidad de Valencia, Burjasot (Valencia), Spain

W. Krause
Max Planck Institut für Festkörperforschung, Heisenbergstrasse 1, D-7000 Stuttgart 80, Federal Republic of Germany

A. Chevy
Laboratoire de Physique des Milieux très Condensés, 4 place Jussieu, Tour 13, quatrième étage, F-75005 Paris, France
(Received 3 October 1983; revised manuscript received 27 February 1984)

Electron scattering mechanisms in n-type indium selenide are investigated by means of the temperature dependence (4—500 K) of Hall mobility and the magnetic field dependence of Hall and magnetoresistance coefficients. The Schmid model for homopolar optical-phonon scattering can explain the temperature dependence of electron mobility above 40 K. The electron-phonon coupling constant is determined, $g^2=0.054$. The optical phonon involved in the process is identified as the A_1' phonon with energy 14.3 meV. The magnetic field dependence of Hall and magnetoresistance coefficients is discussed in terms of the Jones-Zener expansion.

I. INTRODUCTION

Lattice scattering in layered semiconductors has been widely investigated in order to detect the specific features that crystal anisotropy causes in such materials. The temperature dependence of carrier mobility has been measured for several layered compounds such as MoS_2, $MoSe_2$, WSe_2,[1] SnS_2,[2] $SnSe_2$,[3,4] GaS,[5] GaSe,[1,6–8] and InSe.[9–12] In the temperature range through which lattice scattering predominates, the carrier mobility μ changes with absolute temperature T according to a $\mu \propto T^{-\gamma}$ law, with an exponent γ higher than the value $\frac{3}{2}$ corresponding to acoustic-phonon scattering. Fivaz and Mooser,[1] and later Schmid and Fivaz,[13,14] have proposed a model to explain this result. In this model, carriers in layered semiconductors are mainly scattered by homopolar optical phonons polarized along the layer normal. Strong coupling between carriers and homopolar optical phonons arises from the low site symmetry typical of layered structures. With the use of the relaxation-time approximation, the above-mentioned authors calculated the temperature dependence of carrier mobility, and showed that, around a given temperature, it can be expressed in the form $\mu \propto T^{-\gamma}$, the value of the exponent being related to the optical-phonon energy.

Crystal anisotropy further affects carrier scattering. The weakness of binding forces gives rise to a kind of planar defect (stacking faults or interlayer precipitates of impurities) parallel to the layers, which does not affect (or affects very weakly) carrier mobility along the layer $\mu_\perp$ (normal to the c axis), but strongly reduces $\mu_{||}$ (along the c axis).

In the case of InSe, this model was first tested by Atakishiev and Akhundov[9] for n-type material. They found a $\mu_{e\perp} \propto T^{-2}$ law for electron mobility between 300 and 500 K, and deduced an energy of 28 meV for the optical phonon which scatters the electrons. Below 300 K they obtained a $\mu_{e\perp} \propto T^{-3/2}$ law, typical of impurity scattering. Shigetomi *et al.*,[10] by means of Hall and photo-Hall effects in Zn-doped p-type InSe, obtained $\mu_{h\perp} \propto T^{-2.3}$ for hole mobility and $\mu_{e\perp} \propto T^{-1.6}$ for electron mobility between 220 and 330 K. Houdy[11] has found a $\mu_{e\perp} \propto T^{-1.6}$ law for electron mobility in Sn-doped n-type InSe between 100 and 300 K, and has also found that impurity scattering becomes dominant below a temperature of the order of 60 K. Recently, Blasi *et al.*[12] reported a $\mu_{e\perp} \propto T^{-2}$ law in n-type InSe samples and explained this dependence through the interaction of electrons with a 22-meV optical mode.

Electron mobility along the layers, $\mu_{e\perp}$ reaches, in InSe, the highest values among layered semiconductors. Values of the order of 10^3 cm^2/V sec at room temperature[9,11,15] and higher than 10^4 cm^2/V sec at 60 K (Ref. 11) have been reported. Those values are sufficiently high to facilitate the study of the magnetic field dependence of the Hall coefficient.[11]

In this paper we report results on the temperature and magnetic field dependence of electron Hall mobility and the magnetoresistance coefficient in n-type InSe. To our knowledge this is the first time that the magnetoresistance effect is investigated in a layered semiconductor.

Experimental results are presented in Sec. III. The temperature dependence of electron mobility is discussed in Sec. IV in terms of the Schmid model for optical-phonon scattering together with the Brooks-Herring theory of impurity scattering.[16] The magnetic field dependence of Hall and magnetoresistance coefficients is also discussed in Sec. IV using the Jones-Zener expansion.[17]

II. EXPERIMENTAL

The InSe crystals were grown, using the Bridgmann method,[18,19] from a nonstoichiometric melt, $In_{1.12}Se_{0.88}$.

TABLE I. Columns 1, 2, and 3 contain, respectively, list, reference number of the crystal growth, and doping agents of InSe ingots used in this work. Column 4: electron Hall mobility at room temperature (RT). Column 5: maximum value of electron Hall mobility between 4.2 and 500 K. Column 6: absolute temperature at which μ_{max} occurs. Column 7: minus the slope of the double-logarithmic plot of mobility versus temperature at 300 K. Column 8: the same as column 7 at 100 K.

1 InSe ingot	2 Ingot reference no.	3 Doping agent concentration	4 μ_{RT} (cm^2/V sec)	5 μ_{max} (cm^2/V sec)	6 T_m (K)	7 γ_{RT}	8 $\gamma_{100\,K}$
I-a	688/219	Unintentionally doped	620	2×10^4	35	1.7	2.1
I-b	618/172	22 ppm Ga, 42 ppm S	800–1000	4×10^4	25–35	1.7	2.2
I-b[a]	618/172	22 ppm Ga, 42 ppm S	800	1.1×10^4	15	1.6	1.1
I-c	692/222	0.1 at.% Sn	700–900	1.3×10^4	30	1.5	1.6
I-d	722/242	1 at.% Sn	700–900	1.1×10^4	30	1.5	1
I-e	728/246	10 at.% Sn	600–800	1.5×10^3	100	1.4	0
I-f[b]	682/214	0.1 at.% Cd	550	3.2×10^3	60	1.25	1

[a]Annealed 500 °C for 1 h.

[b]Originally strongly compensated p-type InSe, but returned to n-type InSe after annealing at 500 °C for 1 h.

Doping agents, namely SnSe, GaS, etc., were added to the polycrystalline powder. In this work we used samples from the ingots listed in columns 1 and 2 of Table I. The nature and concentration of doping agents are indicated in column 3 of the table. The values indicated there refer to the doping-agent concentration included in the polycrystalline powder. Chemical analysis[19] shows that the actual doping-agent concentration in the InSe monocrystal is much lower due to the high value of impurity segregation coefficients in InSe.[19] A large part of the impurity atoms is rejected towards the end of the ingot, and another part remains in the form of interlayer precipitate planes.[11]

Samples were prepared by cleaving from the ingot with a razor blade. The interference fringe pattern in the infrared transmission spectrum enabled us to measure the thickness of the slabs, which ranged from 5 to 40 μm, the size of the sample being around 5×5 mm^2.

Ohmic contacts for Hall-effect (HE) measurements were made by soldering with high-purity indium. We used the Van der Pauw configuration.[20] The current flows along the layer plane, and therefore, the results here reported only refer to the electron mobility normal to the c axis. Low-temperature HE measurements ($T<300$ K) were carried out with a high-precision automatic apparatus described in Ref. 21.

The sample was immersed in He gas in a cryostat. The maximum magnetic field in this system was $B=0.6$ T. High-temperature HE measurements were performed with a standard system. The sample was heated in vacuum up to 230 °C and the magnetic field was $B=0.3$ T. HE measurements at fixed temperature ($T=77$ K) in a liquid-N_2 immersion cryostat were also carried out. In this case, the maximum magnetic field was $B=2.1$ T. Samples for magnetoresistance measurements were provided with indium-evaporated contacts in Corbino's disk configuration (inset of Fig. 6).

Above 200 K, electron mobility in our InSe samples is smaller than 2×10^3 cm^2/V sec and $\mu^2B^2<0.01$. Therefore our HE results in this temperature range correspond to the low-field limit. Below 100 K, electron mobility is larger than 5×10^3 cm^2/V sec and $\mu^2B^2>0.1$. Low-field conditions are no longer fulfilled. Below 60 K, μ^2B^2 is always larger than 1 and can be as high as 6, which enables us to explore the magnetic field dependence of galvanomagnetic coefficients.

III. RESULTS

A. Temperature dependence of Hall coefficient and electron Hall mobility

In Fig. 1 we have plotted the Hall coefficient R_H versus absolute temperature for one representative sample from each ingot analyzed here. The right ordinate axis represents the electron concentration as calculated from

$$n=1/qR_H\ , \tag{1}$$

where q is the electron charge; we have supposed the Hall

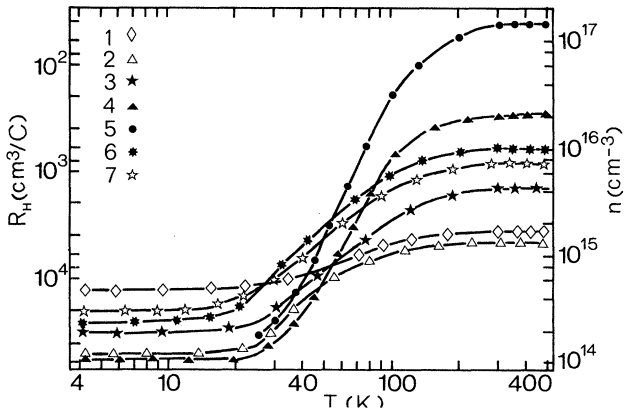

FIG. 1. Hall coefficient versus absolute temperature for several InSe samples from different ingots: unintentionally doped (curve 1), GaS-doped (curve 2), 0.1, 1, and 10 at.% Sn-doped (curves 3, 4, and 5, respectively), 500 °C-annealed GaS-doped (curve 6), and 500 °C-annealed Cd-doped (curve 7) samples.

factor to be 1. This assumption will be discussed in the next section. Discussion about impurity levels has been reported elsewhere.[22] If we examine the behavior of the carrier concentration in these samples (which would be equal to the ionized impurity concentration in noncompensated samples), we can point out several factors necessary for examination of the scattering mechanisms.

(i) Above 300 K, the carrier concentration does not change with temperature in any sample; this means that this temperature range corresponds to the exhaustion region through which all the shallow donors are ionized.

(ii) Below 20 K, the carrier concentration remains constant. This anomalous degeneracy has been discussed elsewhere[22] and has been attributed to the trapping of electrons in two-dimensional accumulation layers created by planar sheets of ionized impurities according to a model proposed by Nicholas *et al.*[23,24]

(iii) Annealing, at 500 °C, of unintentionally doped samples, results in an increase of shallow-donor concentration (curve 6 of Fig. 1) attributed to the diffusion of In atoms from planar interlayer precipitates to interstitial sites where they act as shallow donors.[22] Because of that, originally compensated Cd-doped p-type InSe turns into n-type InSe after annealing at 500 °C (curve 7).

Figures 2 and 3 show the temperature dependence of electron Hall mobility μ_{eH} in several InSe samples from different ingots: GaS-doped ingot I-b (Fig. 2), and Sn-doped ingots I-c, I-d, and I-e (curves 1, 2, and 3, respectively, in Fig. 3). The temperature dependence of μ_{eH} for unintentionally doped and annealed samples is very similar to those shown in Figs. 2 and 3. Quantitative differences are summarized in Table I.

For $T<300$ K, the values of μ_{eH} correspond to $B=0.6$ T, and for $T>300$ K, to $B=0.3$ T. This fact does not modify the results, because for $T>300$ K, low-field-limit conditions are fulfilled and μ_{eH} is independent of B up to $B\sim 2$ T.

We now outline the main features of these results.

(a) The highest values of μ_{eH} occur in GaS-doped InSe (Fig. 2). That occurrence is consistent with the fact that electron-trap concentration is lower than 10^{11} cm^{-3} in those isoelectronically doped samples, as revealed through deep-level transient spectroscopy (DLTS) experiments.[22] We studied GaS-doped samples in which the defect concentration was very low and where the lattice scattering mechanism predominated down to a lower temperature more intensively. In Fig. 4(a) we have plotted the room-temperature mobility for several samples as a function of the room-temperature carrier concentration as calculated with Eq. (1).

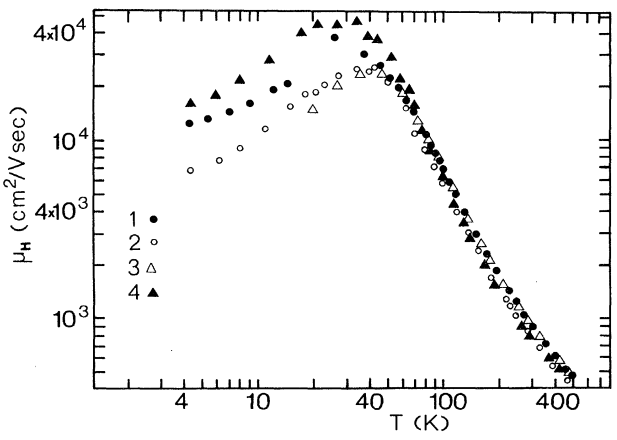

FIG. 2. Hall mobility versus absolute temperature for four samples from the GaS-doped ingot I-b.

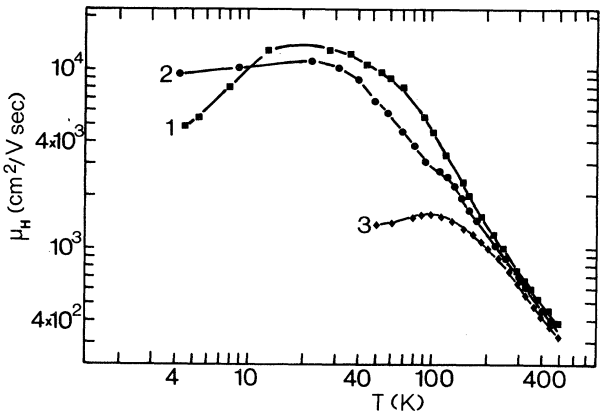

FIG. 3. Hall mobility versus absolute temperature for three samples from the 0.1 at. % (curve 1), 1 at. % (curve 2), and 10 at. % (curve 3) Sn-doped ingots.

(b) Through a temperature interval around a given T_0 (at which $\mu_{eH}=\mu_0$) the electron Hall mobility can be expressed in the form

$$m_{eH}=\mu_0(T_0/T)^{\gamma}\ . \tag{2}$$

The value of γ depends on temperature and doping (Table I, columns 7 and 8). In Fig. 4(b) we have plotted the values of γ at room temperature versus the carrier concentration.

(c) Below T_m the electron Hall mobility monotonically decreases with temperature in each sample, and the results show a larger dispersion than in the high-temperature range, even for samples from the same ingot (Fig. 2).

B. Magnetic field dependence of the Hall coefficient

In the temperature range within which the mobility is high enough to attain $\mu^2B^2\sim 1$, we measured R_H as a function of magnetic field B obtaining a zero-field value R_{H_0} by extrapolating the low-field values in the plot R_H versus B^2. To compare the field dependence at different temperatures we should plot R_H versus $\mu_d^2B^2$, μ_d being the electron drift mobility which is equal to the high-field limit of μ_H. Unfortunately, B was not sufficiently high to reach this limit. We have taken the value of electron Hall mobility μ_{HBm} corresponding to the maximum field attainable, $B_m=0.6$ T. In Fig. 5, R_H/R_{H_0} is plotted versus $\mu_{HBm}^2B^2$ for a high-mobility sample from the GaS-doped ingot at three temperatures. At 4.2 K (curve 1 of the figure), the Hall coefficient is strongly field dependent. At 77 K, R_H does not depend on the magnetic field. Between 4.2 and 77 K, the nonlinearity of the HE

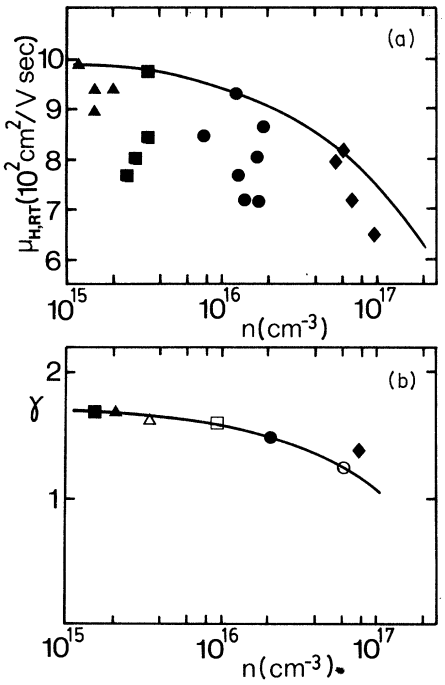

FIG. 4. (a) Hall mobility versus carrier concentration at room temperature for several samples from different ingots: GaS-doped ingot (△), and 0.1 at.% (■), 1 at.% (●), and 10 at.% (◆) Sn-doped ingots. Solid line: electron mobility in function of ionized-impurity concentration, calculated via Eqs. (18), (12), and (29). (b) Minus the slope at room temperature, γ, of the double-logarithmic plot of $\mu(T)$ versus the carrier concentration for several samples: GaS-doped ingot (■), undoped ingot (△), 500°C-annealed GaS-doped ingot (□), 0.1 at.% (△), 1 at.% (●), 10 at.% (○) Sn-doped ingots. and 500°C-annealed Cd-doped (◇) ingot. In the Cd-doped ingot we have also considered the ionized compensating Cd acceptors ($\sim 6\times 10^{16}$ cm^{-3}). Solid line: value of γ versus the ionized-impurity concentration, Eqs. (18), (12), and (29).

becomes less and less significant. In the low-field limit, R_H can be written as

$$R_H(B)=R_{H_0}(1-K_H\mu_{HBm}^2B^2)\ , \tag{3}$$

where K_H is the slope of the curve for $B\rightarrow 0$ and takes the following values: 0.7 at 4.2 K, 0.14 at 40 K, and 0 at 77 K.

C. Temperature and magnetic field dependence of magnetoresistance

Magnetoresistance measurements in Corbino's disk configuration have been carried out. Current I flows radially in the samples (inset of Fig. 6) from central contact 1 to ring contact 4. The voltage measured between contacts 2 and 3 is denoted V_{23}. The relative magnetoresistance is defined in the following manner:

$$\frac{\Delta R(B)}{R(B=0)}=\frac{V_{23}(B)-V_{23}(B=0)}{V_{23}(B=0)}\ , \tag{4}$$

and the magnetoresistance coefficient $H_{\rm mr}$ is[25]

$$H_{\rm mr}=\Delta R/B^2R\ . \tag{5}$$

We can define the magnetoresistance mobility $\mu_{\rm mr}$ as

$$\mu_{\rm mr}=(H_{\rm mr})^{1/2}\ . \tag{6}$$

We have only taken into account the results corresponding to a relative magnetoresistance higher than 2%. Figure 6 shows the temperature dependence of the magnetoresistance mobility in a sample from the GaS-doped ingot I-b, for $B=0.6$ T, between 4.2 and 150 K (curve 1) and for $B=0.8$ T between 4.2 and 80 K (curve 2).

The temperature dependence of $\mu_{\rm mr}$ (for $B=0.6$ T) is very similar to that of μ_H (Fig. 2). The values are of the same order, the maximum occurs at ~ 30 K, and here the $\mu_{\rm mr}\propto T^{-\gamma}$ law is also valid around a given temperature T_0. For $T_0=100$ K we have $\gamma=2.3$, very close to the value $\gamma=2.2$ for Hall mobility in samples from the same ingot at this temperature. The main difference is the magnetic field dependence of the magnetoresistance at the

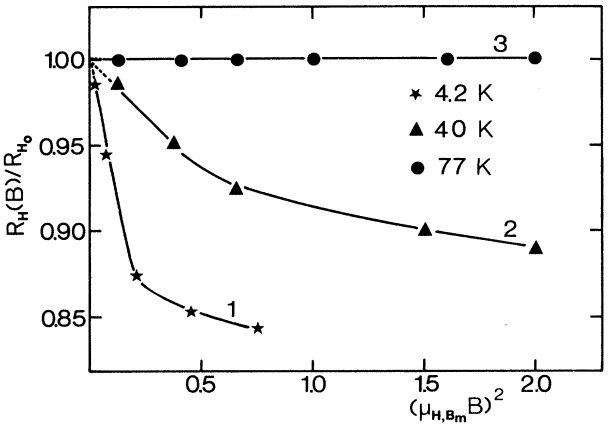

FIG. 5. Ratio of the Hall coefficient for a magnetic field B to its zero-field limit versus the squared product of mobility and magnetic field for a sample from the GaS-doped ingot of 4.2 K (curve 1), 40 K (curve 2), and 77 K (curve 3).

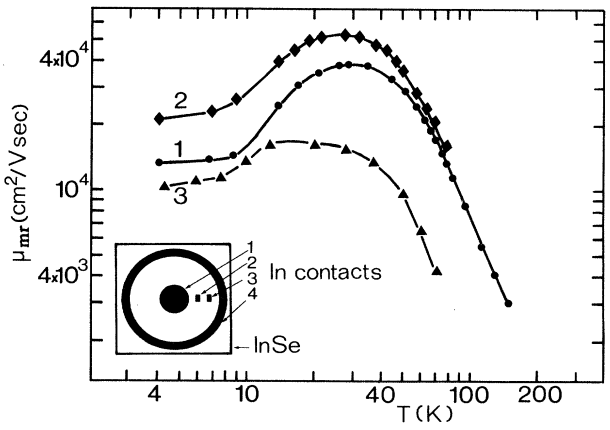

FIG. 6. Electron magnetoresistance mobility versus the absolute temperature for a Corbino-disk sample from the GaS-doped ingot, for $B=0.6$ T (curve 1) and 0.8 T (curve 2).

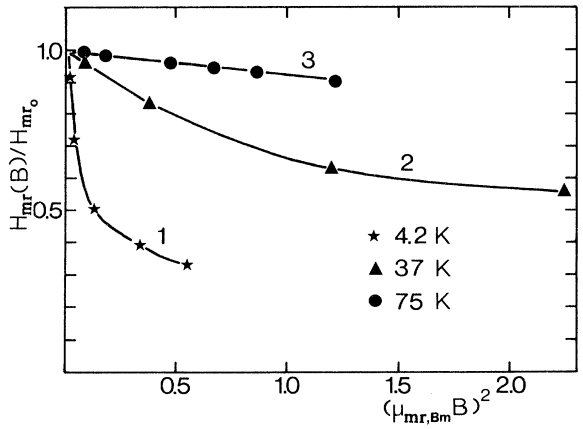

FIG. 7. Ratio of the magnetoresistance coefficient for a magnetic field B to its zero-field limit versus the squared product of mobility and magnetic field in a Corbino-disk sample from the GaS-doped ingot, at 4.2 K (curve 1), 37 K (curve 2), and 75 K (curve 3).

lowest temperature. At 4.2 K, $\mu_{\rm mr}$ is more strongly field dependent than μ_H, but this feature disappears at higher temperatures. In Fig. 6 the ratio between curves 2 and 1 tends to 1 with increasing temperature.

In Fig. 7 we have plotted the magnetic field dependence of the magnetoresistance coefficient. The zero-field value $H_{\rm mr_0}$ is also calculated at each temperature by extrapolating the low-field value. $H_{\rm mr}(B)/H_{\rm mr_0}$ has been plotted versus $\mu^2_{{\rm mr},Bm}B^2$ at three temperatures ($\mu_{{\rm mr},Bm}$ being the magnetoresistance mobility for $B=0.6$ T). At 4.2 K (curve 1 of Fig. 7), $H_{\rm mr}$ is very strongly field dependent, decreasing to 30% of its zero-field value for $B=0.6$ T. From 37 K (curve 2) to 75 K (curve 3), $H_{\rm mr}$ becomes less and less field dependent. For vanishing B, $H_{\rm mr}$ can be expressed in the form

$$H_{\rm mr}(B)=H_{\rm mr_0}(1-K_{\rm mr}\mu^2_{{\rm mr},Bm}B^2)\ , \tag{7}$$

where $K_{\rm mr}$ is the slope of the curve for $B\to 0$. $K_{\rm mr}$ takes the value 7.4 at 4.2 K, 0.4 at 35 K, and 0.08 at 75 K.

Magnetoresistance measurements in HE samples were also performed. Resistivity in absence of magnetic field, ρ_0, increases to ρ_B when a magnetic field B is applied. We can introduce a new magnetoresistance coefficient $H'_{\rm mr}$ (in the presence of the Hall effect, which partially compensates magnetoresistance), which is similar to Eq. (5) and the subsequent magnetoresistance mobility $\mu'_{\rm mr}$. In Fig. 6 (curve 3) we have plotted $\mu'_{\rm mr}$ (for $B=0.6$ T) versus the absolute temperature, as measured in a sample from the GaS-doped ingot, the Hall mobility of which is plotted in Fig. 2 (sample 4). It is interesting to remark that the ratio $\mu'_{\rm mr}/\mu_H$ decreases with increasing the temperature. It is of the order of 0.6 at 4.2 K and goes down to 0.25 at 70 K.

IV. DISCUSSION

A. Theoretical introduction

We now begin the discussion by introducing the physical concepts that we shall use to interpret our results.

According to the Jones-Zener expansion,[17,25] the magnetic field dependence of galvanomagnetic coefficients in the low-field limit is determined by the function which relates relaxation time τ to the electron energy E (in case the relaxation-time approximation applies to the scattering mechanism which we consider). In nondegenerate semiconductors, mean values of the different powers of the relaxation time are defined via

$$\langle\tau^r\rangle=\frac{4}{3\sqrt{\pi}}\int_0^\infty \tau^r(u)e^{-u}u^{3/2}du\ , \tag{8}$$

where $u=E/kT$ and k is the Boltzmann constant. Several factors related to $\tau(E)$ are introduced as follows. We have

$$A_r\equiv\langle\tau^{r+1}\rangle/\langle\tau\rangle^{r+1}\ . \tag{9}$$

The zero-field value of R_H is

$$R_{H_0}=A_1/qn\ , \tag{10}$$

and the low-field value is

$$R_H(B)=R_{H_0}[1-\mu_d^2B^2(A_1^2-2A_2+A_3/A_1)]\ , \tag{11}$$

where μ_d is the drift mobility

$$\mu_d=q\langle\tau\rangle/m^* \tag{12}$$

and m^* is the electron effective mass. The zero-field value of Hall mobility is then

$$\mu_{H_0}=A_1\mu_d\ . \tag{13}$$

The zero-field value of the magnetoresistance coefficient in Corbino's disk configuration (i.e., in absence of the HE) is

$$H_{\rm mr_0}=A_2\mu_d^2\ , \tag{14}$$

and the low-field value is

$$H_{\rm mr}(B)=H_{\rm mr_0}[1-\mu_d^2B^2(A_4/A_2-A_2)]\ , \tag{15}$$

The zero-field value of the magnetoresistance mobility $\mu_{\rm mr_0}$ is then

$$\mu_{\rm mr_0}=(A_2)^{1/2}\mu_d\ . \tag{16}$$

In the presence of the Hall effect, magnetoresistance is, in part, compensated, and we have

$$H'_{\rm mr_0}=(A_2-A_1^2)\mu_d^2\ . \tag{17}$$

We now introduce the relaxation time of the different scattering mechanisms that we shall take into account in our discussion.

(a) Scattering by homopolar optical phonons. In this case, Schmid and Fivaz[13,14] give the following expressions for the relaxation time $\tau_{\rm SF}$:

$$\frac{1}{\tau_{\rm SF}}=\frac{1}{\tau_-}+\frac{1}{\tau_+}\ , \tag{18}$$

$$\frac{1}{\tau_-}=2g^2\omega_{\rm ph}n(E/\hbar\omega_{\rm ph}+1)^{1/2} \tag{19}$$

(phonon-absorption contribution), and

TABLE II. Coefficients which appear in the Jones-Zener expansion (column 1). Theoretical values of these coefficients for an energy-independent (column 2), $E^{-1/2}$-dependent (column 3), and $E^{3/2}$-dependent (column 4) relaxation time. Estimation of the experimental coefficients in high-mobility InSe samples (I-b ingot) at 4.2 K (column 5), 37—40 K (column 6), and 75—77 K (column 7).

1 Scattering mechanism $p=$	2 Low-temperature homopolar optical phonons and neutral impurities 0	3 Acoustic phonons, high-temperature homopolar optical phonons, and low-temperature ionized impurities $-\frac{1}{2}$	4 High-temperature ionized impurities $\frac{3}{2}$	5 Results in this work 4.2 K	6 37—40 K	7 75—77 K
A_1	1	1.18	1.93	~1.2	~1.1	1
$A_1^2-2A_2+A_3/A_1$	0	1.39	615	~0.7	~0.14	0
A_2	1	1.77	5.90	~2	~1	~1
$(A_2)^{1/2}/A_1$	1	1.13	1.26	~1.5	~1	~1
$A_2-A_1^2$	0	0.38	2.18	~0.5	~0.15	<0.05
A_4/A_2-A_2	0	a	18.8	~7.4	~0.4	<0.08

[a]Undetermined; for $p=-\frac{1}{2}$, this coefficient includes $\Gamma(0)$.

$$\frac{1}{\tau_+}=0, \quad E\leq\hbar\omega_{\rm ph}$$
$$\frac{1}{\tau_+}=2g^2\omega_{\rm ph}(n+1)(E/\hbar\omega_{\rm ph}-1)^{1/2}, \quad E>\hbar\omega_{\rm ph} \tag{20}$$

(phonon-emission contribution). g^2 is the electron-phonon coupling constant,

$$g^2=\frac{\epsilon_d^2 m^{*3/2}}{2\sqrt{2}\pi MN\hbar(\hbar\omega_{\rm ph})^{3/2}}, \tag{21}$$

$\hbar\omega_{\rm ph}$ is the energy of the phonon mode, ϵ_d is the deformation potential per unit displacement with respect to the normal coordinate of the phonon mode, M is the reduced ionic mass of the phonon mode, N is the number of cells per unit volume, and n is the phonon occupation number,

$$n=\frac{1}{e^{\hbar\omega_{\rm ph}/kT}-1}. \tag{22}$$

(b) Scattering by ionized impurities. We use the Brooks-Herring relaxation time,

$$\frac{1}{\tau_{\rm BH}}=\frac{N_I q^4 E^{-3/2}}{16\sqrt{2}\pi m^{*1/2}}[\ln(1+b)-b/(1+b)], \tag{23}$$

$$b=\frac{8m^*\epsilon kT}{nq^2\hbar^2}E. \tag{24}$$

N_I is the ionized-impurity concentration, ϵ is the low-frequency dielectric constant of the semiconductor, and n is the free-carrier concentration.

(c) Scattering by neutral impurities. We use the Erginsoy equation,[26]

$$\tau_N=\frac{m^{*2}e^2}{80\pi\epsilon\hbar^2 N_N}, \tag{25}$$

where N_N is the concentration of neutral impurities.

The values of the above-defined different coefficients can be readily obtained, when τ depends on E, via a simple relation $\tau\propto E^p$ where p is an integer or semi-integer number. In Table II we have quoted the values of several coefficients for different values of p. The temperature dependence of the drift mobility can be obtained from Eq. (12) where $\langle\tau\rangle$ is calculated through use of Eq. (8) with $r=1$.

B. Magnetic field dependence of R_H and $H_{\rm mr}$

The quantitative information that can be extracted from our results is somewhat rough because of the limitation of the magnetic field up to 0.6 T. Nevertheless, we can try to take advantage of these results in order to obtain physical conclusions. We shall estimate the experimental values of the coefficients quoted in Table II.

(a) A_1. In Fig. 5 we can see that the slope of curves 1 and 2 decreases with increasing B^2 from their zero-field values (0.7 and 0.14, respectively) to a considerably lower value at the highest field (0.03 and 0.015, respectively). It seems reasonable to plot $R_H(B)/R_{H_0}$ versus $1/B^2$ and to obtain a high-field limit by extrapolating to $B\rightarrow\infty$. The inverse of the value so obtained would be A_1. We obtain $A_1=1.2$ at 4.2 K and 1.1 at 40 K. At 77 K, R_H does not depend on B, and therefore $A_1=1$.

(b) $A_1^2-2A_2+A_3/A_1$. The previous results for the A_1 estimation show that $\mu_{H,Bm}$ differs from high-field limit μ_d by less than 2%. Thus, we can identify K_H in Eq. (3) with $A_1^2-2A_2+A_3/A_1$ with an error of the order of 4%.

(c) A_2. We can guess this factor by the ratio of $H_{\rm mr_0}$ to $\mu_{H,Bm}^2$.

(d) $(A_2)^{1/2}/A_1$. It may be identified to the ratio $\mu_{\rm mr_0}/\mu_{H_0}$.

(e) $A_2-A_1^2$. We can obtain this coefficient through the ratio $H'_{\rm mr_0}/\mu_{H,Bm}^2$, or calculate it directly from the estimated values of A_1 and A_2. Both methods yield values of the same order.

(f) A_4/A_2-A_2. With the same accuracy, this factor can be identified with $K_{\rm mr}$ in Eq. (7).

In columns 5, 6, and 7 of Table II, we have quoted the values so obtained at 4.2, 37—40, and 75—77 K, respectively. At 4.2 K, those values are close to the theoretical

ones for $p=-\frac{1}{2}$, which could be explained by the low-temperature form of the impurity-scattering relaxation time. Nevertheless, this result must be used with caution, as it concerns electrons trapped in two-dimensional accumulation layers.[23,24] The lack of information about size and concentration of these defects does not permit definitive conclusions.

At 75–77 K, all of the coefficients seem to correspond to an energy-independent relaxation time—this can also be the case for homopolar optical scattering in the low-temperature limit. The electron energy would be very small with respect to $\hbar\omega_{\rm ph}$, and the relaxation time would be

$$\tau_{\rm SF}=\tau_{-}=(2g^2\omega_{\rm ph}n)^{-1}\ . \tag{26}$$

Fivaz and Schmid[14] have also shown that in a two-dimensional model of a layered semiconductor, with a two-dimensional electron density of states, the relaxation time for homopolar optical scattering does not depend on electron energy. Nevertheless, band-structure calculations[27] and cyclotron-resonance measurements[23,24] exclude this possibility for InSe, which has a three-dimensional band structure.

At 37–40 K, the values of the coefficients are intermediate between the ones for $p=-\frac{1}{2}$ and those for $p=0$, which may indicate the presence of both scattering mechanisms. A dominance of impurity scattering at high temperatures must be excluded. The theoretical values of column 4 in Table II are very different from the experimental ones at any temperature.

C. Temperature dependence of electron mobility

The temperature dependence of the drift mobility can be theoretically calculated through Eqs. (8) and (12). Hall mobility would be obtained via Eq. (13) after determining the dominant scattering mechanism. The magnetic field dependence of R_H and $H_{\rm mr}$ indicates that homopolar–optical-phonon scattering dominates above 77 K. At 77 K, we have obtained $A_1=1$. At the highest temperature the electron mobility is low and a magnetic field as high as 10 T would be necessary to obtain A_1. Taking into account that the high-temperature limit of $\tau_{\rm SF}$ is proportional to $E^{-1/2}$, A_1 would change between 1 (at $kT\ll\hbar\omega_{\rm ph}$) and 1.18 (at $kT\gg\hbar\omega_{\rm ph}$). The change that this correction would introduce in the slope of the double-logarithmic plot of mobility versus temperature is sufficiently low to be neglected. In the low-temperature range, where impurity scattering dominates, we have seen that A_1 varies between 1.2 and 4.2 K and 1.1 at 40 K. The dispersion of results of this temperature range allows us to neglect the correction. Therefore, we can consider $A_1=1$ in the entire temperature range without losing physical information.

We shall begin interpreting the results in the high-temperature range using the Schmid-Fivaz model. In order to calculate $\mu_d(T)$ with $\tau_{\rm SF}$, two parameters must be determined, the phonon energy $\hbar\omega_{\rm ph}$ and the electron-phonon coupling constant g^2. The electron effective mass in InSe has been determined by Portal *et al.*,[28,23,24]

$$m_{\perp}^{*}=0.131m_0,\quad m_{\parallel}^{*}=0.081m_0\ ,$$

where m_0 is the electron mass.

Through Raman measurements,[29–31] two homopolar optical phonons with A_1' symmetry and polarization vectors normal to the layers have been detected in InSe. The energies of these phonons are $\hbar\omega_1=14.3$ meV and $\hbar\omega_2=27.8$ meV. Displacement vectors are shown in the inset of Fig. 8. Instead of considering $\hbar\omega_{\rm ph}$ as a fitting parameter, we shall start calculating $\mu_d(T)$ with $\tau_{\rm SF}$ for both phonon energies, and then compare these results with experimental results. Therefore, the only setting parameter is the coupling constant g^2, which can be chosen so as to obtain the highest value of electron mobility at room temperature. Afterwards, we will introduce the impurity scattering and verify if it changes the calculated room-temperature mobility.

The highest measured value of electron mobility at 300 K is 980 cm^2/V sec. To obtain this value with Eqs. (8), (12), and (18), we must set $g^2=0.06$ for $\hbar\omega_{\rm ph}=14.3$ meV and $g^2=0.10$ for $\hbar\omega_{\rm ph}=27.8$ meV. In Fig. 8 we have plotted the calculated $\mu_d(T)$ for $\hbar\omega_{\rm ph}=14.3$ meV (curve 1) and $\hbar\omega_{\rm ph}=27.8$ meV (curve 2). Curve 2 does not fit the experimental results at all. The slope of this curve at 300 K is 2.3, considerably higher than experimental value, 1.7. On the other hand, curve 1 perfectly reproduces the experimental results between 120 and 500 K, but departs from it below 120 K, which can be explained by the presence of impurity scattering. This mechanism (as well as neutral impurities, dislocations, etc.) may also work at room temperature. Therefore, the highest measured value of electron mobility may be lower than the "intrinsic" electron mobility (i.e., the electron mobility limited only by lattice scattering). In Fig. 6(a) the effect of doping on room-temperature mobility clearly appears. Thus, we shall introduce the impurity scattering through the

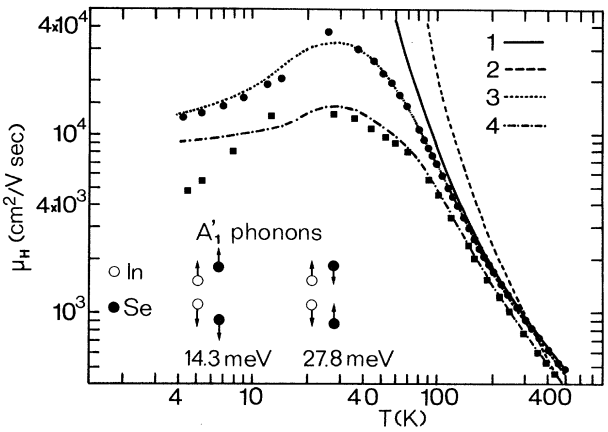

FIG. 8. Comparison between experimental and calculated $\mu(T)$. Experimental points: one sample from the GaS-doped ingot (●) and another from the 0.1 at.% Sn-doped ingot (■). Curve 1: calculated mobility for the Schmid relaxation time with $g^2=0.06$ and $\hbar\omega_{\rm ph}=14.3$ meV. Curve 2: calculated mobility for the Schmid relaxation time with $g^2=0.1$ and $\hbar\omega_{\rm ph}=27.8$ meV. Curve 3: calculated mobility for the relaxation time given by Eq. (29) with $g^2=0.054$, $\hbar\omega_{\rm ph}=14.3$ meV, $N_1=2\times10^{14}$ cm^{-3}, and $N_2=1.5\times10^{15}$ cm^{-3}. Curve 4: the same as curve 3 with $N_1 5\times10^{14}$ cm^{-3} and $N_2=5\times10^{15}$ cm^{-3}.

Brooks-Herring relaxation time, and recalculate μ_d at room temperature with

$$1/\tau = 1/\tau_{SF} + 1/\tau_{BH} . \tag{27}$$

The low-frequency dielectric constant of InSe is anisotropic ($\epsilon_{||}=9.9$ and $\epsilon_{\perp}=10.9$).[32] Taking the mean value $\epsilon=(\epsilon\epsilon_{\perp}^2)^{1/3}=10.6$ and making N_I equal to the room-temperature carrier concentration in GaS-doped samples, $n=1.5\times10^{15}$ cm^{-3}, the calculated value of μ_d at room temperature decreases to 800 cm^2/V sec. In order to obtain the experimental value with both scattering mechanisms, we must take a longer coupling constant, $g^2=0.054$.

We have calculated the room-temperature mobility as a function of N_I. We suppose $N_I=n$, which is true at room temperature in noncompensated samples. The calculated $\mu_d(N_I)$ is plotted in Fig. 4(a), and fits the highest values of measured electron mobility for each carrier concentration.

To obtain $\mu_d(T)$ we must introduce a new hypothesis in our model. The carrier concentration and, therefore, the ionized-impurity concentration, changes with temperature as plotted in Fig. 1. The experimental curve $n(T)$ can be reproduced through a phenomenological model. Two impurity levels are supposed to exist in InSe.[22] One of them, with zero ionization energy, remains ionized even at the lowest temperature, and its concentration is N_1. The other has an ionization energy E_{d2} and a concentration N_2. The carrier concentration can be expressed as a function of temperature,[22]

$$n(T)=\tfrac{1}{4}\{[N_c\exp(-E_{d2}/kT)-2N_1]^2+8N_c(N_1+N_2)\exp(-E_{d2}/kT\}^{1/2}-\tfrac{1}{4}[N_c\exp(-E_{d2}/kT)-2N_1] . \tag{28}$$

$N_c=2(m_d^* kT/2\pi h^2)^{3/2}$ is the effective density of states in the conduction band and $m_d^*=(m_{||}^* m_{\perp}^{*2})^{1/3}$. The ionization energy is 18.5 meV in undoped samples and 44 meV in Sn-doped samples.[22]

We also take into account the scattering effect of neutral impurities, supposing that the only neutral impurities in the sample arise from the freezing out of electrons in the donor levels. Therefore, the concentration of neutral impurities is

$$N_N = N_1 + N_2 - n .$$

We can now calculate $\mu_d(T)$ with a relaxation time, taking into account the three contributions,

$$1/\tau = 1/\tau_{SF} + 1/\tau_{BH} + 1/\tau_N , \tag{29}$$

where τ_N is given by Eq. (25).

In Fig. 8 we have plotted the calculated $\mu_d(T)$ for the relaxation time given by Eq. (29) for one undoped sample ($E_{d2}=18.5$ meV). The best fit to the experimental results for sample 1 of the GaS-doped ingot (Fig. 2), taken here as representative, is obtained for $N_1=2\times10^{14}$ cm^{-3} and $N_2=1.5\times10^{15}$ cm^{-3} (curve 3 of Fig. 8).

We have also applied this model to interpret the results on 0.1 at. % Sn-doped samples, the experimental points of which are reproduced in Fig. 8. Curve 4 in this figure has been calculated taking $E_{d2}=44$ meV, $N_1=5\times10^{14}$ cm^{-3}, and $N_2=5\times10^{15}$ cm^{-3}. The fit is good in the high-temperature range, but it fails at low temperature. The model also fails for highly doped samples (1 and 10 at. % Sn- and Cd-doped InSe); this may be due to the presence of acceptor levels which remains ionized even at the lowest temperature. That is true for intentionally Cd-doped InSe which contains $\sim10^{16}$ Cd acceptors per cm^3. In the case of 10 at. % Sn-doped samples, acceptors may be present from residual impurities contained in tin. We have also calculated the value of exponent γ at room temperature as a function of the ionized-impurity concentration [solid curve in Fig. 4(b)].

In conclusion, homopolar—optical-phonon scattering predominantly determines the electron mobility between 120 and 500 K. Our results show that impurity scattering is also present in this temperature range. It reduces the electron mobility and the exponent γ present in Eq. (2), which enabled us to interpret the experimental results without taking the phonon energy as a fitting parameter, but using instead the measured value of $\hbar\omega_{ph}$.

Our results are consistent with Bourdon's band-structure calculation of InSe,[27] which shows that the uppermost valence band and the lowest conduction band are mainly determined by the In—In bond and antibonding orbitals. The 14.3-meV A_1' phonon strongly stretches the In—In bond and must be coupled to electrons. The 27.8-meV mode also stretches this bond, but the coupling constant inversely depends on phonon energy and must be lower.

Schmid and Fivaz[13,14] also show that electron-phonon interaction is responsible for the main part of the temperature dependence of the energy gap in layered semiconductors. Camassel *et al.*[33] have shown that the temperature dependence of the InSe gap, as well as the broadening of the exciton-absorption peak, can be accounted for by the coupling of electrons with a 14-meV homopolar phonon, which confirms our results. Nevertheless, the coupling constant determined by these authors, $g^2=0.25$, differs from our results. If we let $g^2=0.25$, the electron mobility at room temperature will be of the order of 230 cm^2/V sec, which is less than one-fourth of the electron mobility in the GaS-doped ingot. This contradiction may be explained by the fact that the valence band also takes part in the temperature dependence of the gap, as well as in the broadening of the exciton-absorption peak. The value $g^2=0.25$ may correspond to the valence band. The value $g^2=0.054$, determined from electron mobility, is clearly associated with the conduction band.

In the case of GaSe, Schmid and Voitchotsky[6] found nearly the same temperature dependence for electrons and holes ($\mu_e \propto T^{-2}$ and $\mu_h \propto T^{-1.9}$). The electron-phonon coupling constant has the same value, $g^2=0.25$, whether it is obtained from transport measurements or from the temperature dependence of the gap. They conclude that the main contribution to the temperature dependence of

the gap comes from the valence band. This also seems to occur in InSe. Nevertheless, Shigetomi *et al.*[10] found, in Zn-doped p-type InSe samples, different temperature laws for electron and hole mobilities ($\mu_e \propto T^{-1.6}$ and $\mu_h \propto T^{-2.3}$ between 220 and 330 K). The slope of curve 2 in Fig. 8 at room temperature is 2.3. In the Schmid model it would mean that holes in InSe are scattered by the 27.8-meV A_1' phonon. In Bourdon's InSe band-structure calculations, the absolute maximum of the valence band is not at the Γ point. The maximum is 20 meV higher than the Γ extremum and also has a contribution from the In—Se bond. The 27.8-meV A_1' phonon, which also stretches the In—Se bond, could be more strongly coupled with holes than the 14.3-meV mode. Unfortunately, the coupling constant for holes cannot be accurately obtained since no direct measurements of the hole effective mass are available. The hole mobility in InSe is $\mu_{h\perp} \sim 30$ cm^2/V sec[10,11,15,19] To obtain this value in the Schmid model, we must allow $m_h^* g_h^2/m_0 = 0.43$. Taking $g_h^2 = 0.25$,[33] we would obtain $m_h^* = 1.7 m_0$, which lies below the values calculated by Bourdon ($5m_0$ at the Γ point and $8m_0$ at the absolute maximum of the conduction band).

D. Magnetoresistance

The behavior of the magnetoresistance mobility μ_{mr} in the temperature range through which we could perform accurate measurements is nearly the same as μ_H. This is made clear in our discussion of the Jones-Zener expansion. We have seen that over the entire temperature range, the Hall factors A_1 and A_2 are very close to unity. Therefore, the magnetoresistance mobility is very close to μ_H and shows the same temperature dependence.

V. CONCLUSIONS

The results reported here confirm the validity of the Schmid model for homopolar—optical-phonon scattering in layered semiconductors. The temperature dependence of electron mobility in undoped n-type InSe above 120 K can be explained by the coupling of electrons with a 14.3-meV phonon which may be identified as the low-energy A_1' phonon. This process has also been proposed to explain the temperature dependence of the gap in InSe.[33] We have also determined the electron-phonon coupling constant $g^2 = 0.054$ which differs from the value $g^2 = 0.25$ given in Ref. 33 from optical measurements. Our result clearly corresponds to the conduction band. Therefore, the value 0.25 should be associated with the valence band.

To give an exact account of the room-temperature mobility and the exponent γ which appears in the $\mu \propto T^{-\gamma}$ law, we have also taken into account the ionized- and neutral-impurity scattering, and calculated the electron mobility and exponent γ as a function of the impurity concentration.

The magnetic field dependence of the Hall and magnetoresistance coefficients are able to be explored due to the high value of electron mobility in InSe. Using the Jones-Zener expansion, we could interpret the results showing that, by increasing the temperature, the dominant scattering mechanism changes from one with a strongly energy-dependent relaxation time at 4.2 K (impurity scattering) to one with a smoothly energy-dependent relaxation time at 77 K (homopolar—optical-phonon scattering). This fact also explains that increasing the temperature increases the linearity of the Hall effect (for identical values of $\mu^2 B^2$). It also explains the similarity of Hall and magnetoresistance mobilities.

ACKNOWLEDGMENTS

The low-temperature experiments were performed at the Max-Planck-Institut für Festkörperforschung, Stuttgart. One of the authors (A.S.) wishes to thank Professor H. J. Queisser for his hospitality and support during his stay at the Max-Planck-Institut.

[1] R. Fivaz and E. Mooser, Phys. Rev. 163, 743 (1967).
[2] J. P. Gowers and P. A. Lee, Solid State Commun. 4, 1447 (1970).
[3] B. L. Evans and R. A. Hazelwood, J. Phys. D 2, 1507 (1969).
[4] A. I. Likhter, E. G. Pel, and S. I. Prysyazhnyuk, Phys. Status Solidi A 14, 265 (1972).
[5] A. H. Kipperman and C. J. Vermig, Nuovo Cimento 63B, 29 (1969).
[6] Ph. Schmid and J. P. Voitchovsky, Phys. Status Solidi B 65, 249 (1974).
[7] C. Manfredotti, A. M. Mancini, R. Murri, A. Rizzo, and L. Vasenelli, Nuovo Cimento 39B, 257 (1977).
[8] V. Augelli, C. Manfredotti, R. Murri, and L. Vasenelli, Phys. Rev. B 17, 3221 (1978).
[9] S. M. Atakishiev and G. A. Akhundov, Phys. Status Solidi 32, K33 (1969).
[10] S. Shigetomi, T. Ikari, Y. Koga, and S. Shigetomi, Jpn. J. Appl. Phys. 20, L343 (1981).
[11] P. Houdy, Thèse de Troisième Cycle, Université de Paris VII, 1982.
[12] C. De Blasi, G. Micocci, A. Rizzo, and A. Tepore, Phys. Rev. B 27, 2429 (1983).
[13] Ph. Schmid, Nuovo Cimento 21B, 258 (1974).
[14] R. Fivaz and Ph. Schmid, *Optical and Electrical Properties* (Reidel, Dordrecht, The Netherlands, 1976), p. 385.
[15] A. Segura, J. P. Guesdon, J. M. Besson, and A. Chevy, J. Appl. Phys. 54, 876 (1983).
[16] H. Brooks, *Advances in Electronics and Electron Physics* (Academic, New York, 1955), Vol. 7, p. 85.
[17] H. Jones and C. Zener, Proc. R. Soc. London, Ser. A 144, 101 (1934).
[18] A. Chevy, A. Kuhn, and M. S. Martin, J. Cryst. Growth 38, 18 (1977).
[19] A. Chevy, these d'etat, Université de Paris VI, 1982.
[20] L. J. Van der Pauw, Philips Res. Rep. 13, 1 (1955).
[21] P. Hiesinger, diploma thesis, University of Frankfurt, 1971.
[22] A. Segura, K. Wünstel, and A. Chevy, Appl. Phys. 31A, 139, (1983).
[23] R. J. Nicholas, E. Kress-Rogers, J. C. Portal, J. Galibert, and A. Chevy, Surf. Sci. 113, 339 (1982).
[24] E. Kress-Rogers, R. J. Nicholas, J. C. Portal, and A. Chevy, Solid State Commun. 44, 379 (1982).

[25]P. Kireev, *La Physique des Semiconducteurs* (Mir, Moscow, 1975).

[26]C. Erginsoy, Phys. Rev. 79, 1013 (1950).

[27]A. Bourdon, A. Chevy, and J. M. Besson, in *Proceedings of the 14th International Conference on the Physics of Semiconductors, Edinburgh, 1978,* edited by B. L. H. Wilson (IOP, Bristol, 1978), p. 1371.

[28]J. C. Portal, R. J. Nicholas, E. Kress-Rogers, A. Chevy, J. M. Besson, J. Galibert, and D. Perrier, in Proceedings of the 15th International Conference on the Physics of Semiconductors, Kyoto, 1980 [J. Phys. Soc. Jpn. Suppl. A 49, 879 (1980)].

[29]S. Jandl and C. Carlone, Solid State Commun. 25, 5 (1978).

[30]N. M. Gasalny, B. M. Yavadov, V. I. Tagirov, and E. A. Vinogradov, Phys. Status Solidi B 89, K43 (1978).

[31]F. E. Faradev, N. M. Gasalny, B. N. Mavrin, and N. M. Melnik, Phys. Status Solidi B 85, 381 (1978).

[32]N. Kuroda and Y. Nishima, Solid State Commun. 34, 481 (1980).

[33]J. Camassel, P. Merle, H. Mathieu, and A. Chevy, Phys. Rev. B 17, 4718 (1978).